Terahertz imaging of sub-wavelength particles with Zenneck surface waves

M. Navarro-Cía, M. Natrella, F. Dominec, J. C. Delagnes, P. Kužel, P. Mounaix, C. Graham, C. C. Renaud, A. J. Seeds, and O. Mitrofanov

Citation: Applied Physics Letters **103**, 221103 (2013); doi: 10.1063/1.4836195
View online: http://dx.doi.org/10.1063/1.4836195
View Table of Contents: http://scitation.aip.org/content/aip/journal/apl/103/22?ver=pdfcov
Published by the AIP Publishing

Terahertz imaging of sub-wavelength particles with Zenneck surface waves

M. Navarro-Cía,[1,2,3,4,a)] M. Natrella,[4] F. Dominec,[5] J. C. Delagnes,[6] P. Kužel,[5,b)] P. Mounaix,[6,c)] C. Graham,[4] C. C. Renaud,[4] A. J. Seeds,[4] and O. Mitrofanov[4,d)]
[1]*Optical and Semiconductor Devices Group, Department of Electrical and Electronic Engineering, Imperial College London, London SW7 2BT, United Kingdom*
[2]*Centre for Plasmonics and Metamaterials, Imperial College London, London SW7 2AZ, United Kingdom*
[3]*Centre for Terahertz Science and Engineering, Imperial College London, London SW7 2AZ, United Kingdom*
[4]*Department of Electronic and Electrical Engineering, University College London, Torrington Place, London WC1E 7JE, United Kingdom*
[5]*Institute of Physics, Academy of Sciences of the Czech Republic, Na Slovance 2, 182 21 Prague 8, Czech Republic*
[6]*LOMA, Bordeaux 1 University, CNRS UMR 4798, 351 cours de la Libération, 33405 Talence, France*

(Received 3 August 2013; accepted 11 November 2013; published online 25 November 2013)

Impact of sub-wavelength-size dielectric particles on Zenneck surface waves on planar metallic antennas is investigated at terahertz (THz) frequencies with THz near-field probe microscopy. Perturbations of the surface waves show the particle presence, despite its sub-wavelength size. The experimental configuration, which utilizes excitation of surface waves at metallic edges, is suitable for THz imaging of dielectric sub-wavelength size objects. As a proof of concept, the effects of a small strontium titanate rectangular particle and a titanium dioxide sphere on the surface field of a bow-tie antenna are experimentally detected and verified using full-wave simulations. [http://dx.doi.org/10.1063/1.4836195]

Antennas are extensively used to enhance the coupling between free-space propagating waves and electronic devices.[1] Recently, the use of antennas has been extended toward higher frequencies where they have found applications in other fields, such as energy harvesting, nonlinear optics, and quantum physics.[2] Upon high frequency excitation (typically beyond microwaves), metallic antennas cannot be described by electric currents only. In the terahertz (THz) range, Zenneck THz surface waves (Z-TSWs), which produce the main contribution in the near-field region of the antenna, also need to be considered. In this description, antennas convert the incident free-space electromagnetic wave into surface waves.

The effect of Z-TSW excitation on THz bow-tie antennas has been recently discussed and observed experimentally with an integrated sub-wavelength aperture THz near-field (NF) probe.[3,4] In this THz microscopy system, a flat metallic surface with a small aperture is interacting with the antenna. It was found that placing the metallic plane of the probe close to a surface, which supports a Z-TSW, enhances the field of this wave (by of factor of 10 for a 3 μm separation between antenna and the probe) whereas the wave properties (the angular distribution of wave vectors) remain determined by the supporting surface geometry and stay practically unaffected by the metallic plane of the probe.[4] This configuration, consisting of a planar antenna and the metallic plane of the NF probe placed parallel to the antenna plane, offers a possibility for THz imaging and spectroscopy of small (sub-wavelength size) dielectric objects.

Consider a sub-wavelength size dielectric particle positioned between the metallic antenna surface and the probe surface. The enhancement of the Z-TSW produced in this configuration causes stronger coupling of the THz wave to the particle. The particle, in its turn, distorts the Z-TSW field pattern on the bow-tie antenna. The distortion reflects the geometrical properties of the particle and its polarizability. The effect can be understood as Mie scattering by a single particle.[5] On the other hand, the field distortion is the underlying reason for a change in the antenna frequency response due to the particle.

The NF probe allows mapping the field distortion caused by the particle. Consequently, geometrical properties of the particle, its location, polarizability, and even its ability to confine the electromagnetic field can be determined in this configuration. Note that the field enhancement between the surfaces of the antenna and the probe helps detecting particles, which otherwise would be almost invisible to THz radiation.

Surface-confined waves have already been proposed and exploited for THz spectroscopic analysis.[6–14] Parallel plate waveguides filled with dielectrics were shown to increase the technique's sensitivity by confining THz waves only to the sub-wavelength size region between the plates.[6] The sensitivity to small objects can be increased further by inserting a resonant cavity[7] or by adiabatic tapering of the waveguide plates.[8–10] THz field confinement to extremely small volumes can be achieved by a twin-needle probe,[11] by planar transmission lines, which can be used for on-chip THz spectroscopy,[12,13] and by long narrow slits.[14]

More traditional THz spectroscopy with focused (diffraction-limited) THz beams has also been applied to sub-wavelength size objects. The spatial selectivity was achieved by attaching the sample under test to a metallic screen with a sub-wavelength aperture (as small as 10 μm)[15] or by placing the sample on an electro-optic crystal

[a)]Electronic mail: m.navarro@imperial.ac.uk
[b)]Electronic mail: kuzelp@fzu.cz
[c)]Electronic mail: p.mounaix@loma.u-bordeaux1.fr
[d)]Electronic mail: o.mitrofanov@ucl.ac.uk

directly.[16,17] The spatial resolution in the latter case is of the order of several tens of μm, determined by the electro-optics crystal thickness.[16,17]

Here we investigate the interaction of Z-TSWs with sub-wavelength size dielectric particles placed between a THz planar antenna and a metallic plane. We demonstrate that near-field mapping of the surface field enables direct detection of the particles. The experimental configuration discussed here can enable high-resolution THz imaging of sub-wavelength size objects in addition to the spectroscopic analysis. Our experimental results are supported by three-dimensional full-wave numerical calculations.

We consider particles made of two materials: strontium titanate $SrTiO_3$ (STO) used in electrically tuneable structures,[18,19] which exhibits a strong polar soft mode at THz frequencies, and titanium dioxide (TiO_2), which exhibits a large value of the dielectric constant.[20,21] Both kinds of particles were shown to exhibit Mie resonances in the THz range with a strong effective magnetic response.[21,22] Such high-permittivity dielectric particles of sub-wavelength size are building blocks for THz dielectric metamaterials.[22] Direct measurements of near-field interaction of the electromagnetic field with single particles can provide essential characteristics of the particles, crucial for validation of numerical simulations.

The time-domain NF microscopy system used is shown in Fig. 1 (details are described in Refs. 3, 23, and 24). For the excitation of surface waves on the antenna, THz pulses generated *via* optical rectification in ZnTe are directed on the bow-tie sample using 80 mm long cylindrical metallic waveguides of diameter Ø1 or 1.6 mm.[25] The bow-tie antenna is fabricated by optical lithography using a 300 nm thick gold (Au) layer deposited on a GaAs substrate. The bow-tie has 300 μm long arms with an angle of 90°. The THz beam is comparable to the bow-tie size as it is shown in Fig. 2. A sub-wavelength size particle is attached to the surface of one of the bow-tie arms and the sample is scanned (together with the output end of the waveguide) with respect to an integrated sub-wavelength aperture THz NF probe.[3,4,26,27] The THz NF probe has an aperture of $d = 10\,\mu$m and an integrated photoconductive antenna detector.[23,27] The overall spatial resolution of this NF probe is determined by the aperture size and the distance to the sample. When the NF probe-sample separation is less than $d/3$ and thus the evanescent fields of high spatial frequency can be collected by the NF probe, the spatial resolution equals approximately the aperture size d.[23] The probe can detect THz surface waves as well as the incident THz wave, producing a sum of two signals: one is proportional to the temporal derivative of the horizontally polarized electric field (E_x) of the incoming THz pulse[28] and the other is proportional to the spatial derivative of the out-of-plane electric field (dE_z/dx) of the Z-TSW.[3,4,26] In the area of the bow-tie antenna, where the incident THz wave is blocked by the metal, only the contribution of the Z-TSW, dE_z/d_x, remains. Typical detected surface wave patterns on plain bow-tie antennas can be found in Refs. 3 and 4.

In our first experiment, a rectangular dielectric particle, made of STO with approximate dimensions of 55 μm $\times$ 95 μm $\times$ 25 μm (width $\times$ length $\times$ height), is positioned on the right-hand side of the bow-tie, covering $\sim$1/10 of the arm area (top inset in Fig. 2(a)). The electric permittivity of STO (at $T = 300$ K) is $\varepsilon_r \sim 300$ at THz frequencies,[29] resulting in the fundamental resonance within the particle at $f_r \sim 0.4$ THz when it is illuminated by a plane-wave polarized along the height of the particle.

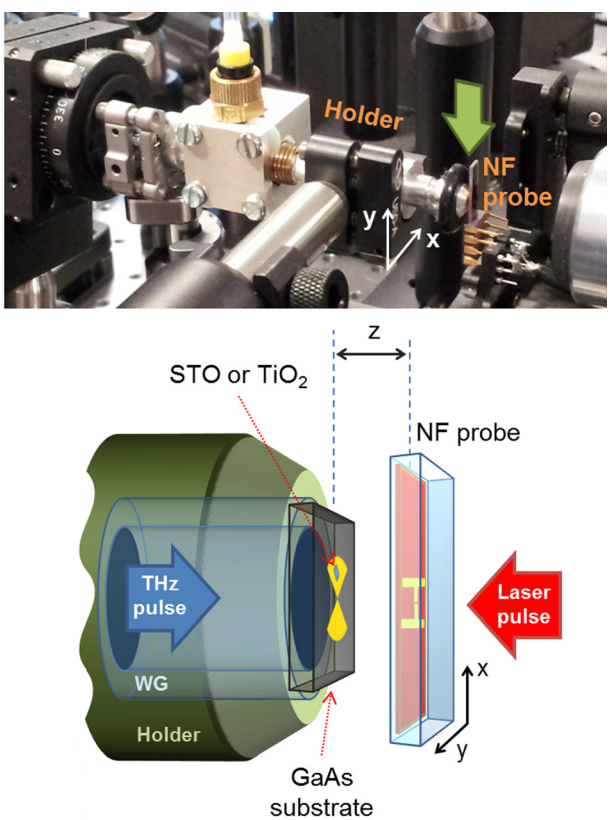

FIG. 1. (top) Photograph of the experimental setup. The green arrow indicates the region magnified in the bottom sketch. (bottom) Sketch of the sample and NF probe. The origin of the coordinate system is considered the centre of the bow-tie antenna.

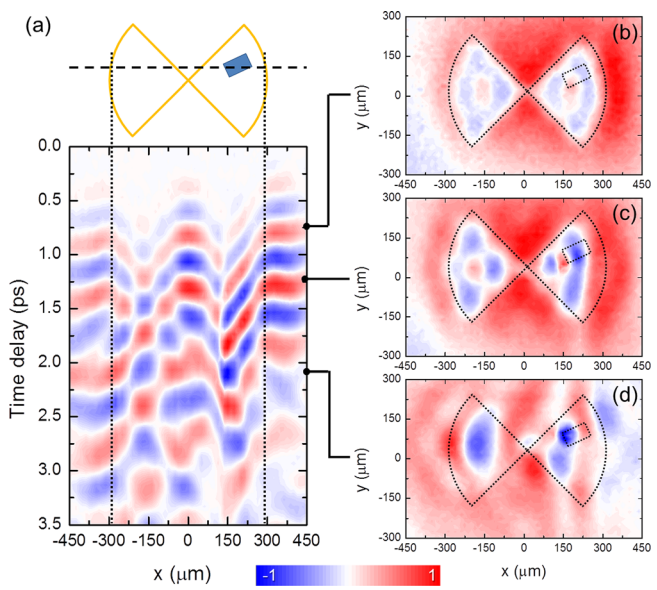

FIG. 2. (a) Measured temporal evolution of the detected signal along the horizontal line outlined in the diagram at $z \sim 25\,\mu$m. (b)-(d) THz near-field images for selected time delays indicated on the xt-map. The bow-tie and the STO particle are outlined with dotted lines.

Spatial *xy*-maps of the field in the vicinity of the sample are measured at different distances z of the probe from the bow-tie surface to ensure that the field mapping is done at the closest sample-probe separation. Space-time maps[3] are recorded to confirm surface wave excitation at the bow-tie edges. Fig. 2(a) shows an *xt*-map along the horizontal line scan passing through the middle of the STO particle for $z \sim 25\ \mu$m (the STO particle is within ~1–3 μm from the probe surface). The temporal evolution of the field in the area of the bow-tie shows excitation of Z-TSWs. In this map, the incident THz pulse is also present at $|x| > 300\ \mu$m and at $|x| < 50$, in the regions where the bow-tie does not block the wave, for t within the interval 0.5–2.0 ps.

At $t \sim 0.5$ ps, the Z-TSWs only start to develop at the edges of the bow-tie and there is still no signal detected within the bow-tie arms. At $t \sim 0.75$ ps, the Z-TSWs become noticeable and the corresponding *xy*-map shows a symmetric pattern within the bow-tie (Fig. 2(b)). As time progresses, the Z-TSWs propagate away from the antenna edges towards the centre of each arm, generating a characteristic pattern in the *xt*-map: the wavefronts become tilted in the space-time maps corresponding the wave propagation along the metallic surfaces. The Z-TSWs reach the STO particle (outlined in Fig. 2) at $t \sim 0.75$ ps initiating the interaction with the STO particle.

The interaction between the surface wave and the STO particle is illustrated in Figs. 2(b)–2(d). At $t \sim 0.75$ ps (Fig. 2(b)), the particle shows practically no effect on the Z-TSWs and the field pattern is symmetric.[3,4] The surface wave fully develops within the bow-tie in the following picosecond. At $t \sim 1.25$ ps (Fig. 2(c)), the symmetry of the bow-tie pattern is broken. The left arm retains the pattern similar to field observed on a clean bow-tie,[3,4] but the pattern on the right arm is largely affected. At $t \sim 2.1$ ps the field perturbation becomes very clear (Fig. 2(d)) as the field inside the bow-tie region is noticeably larger than outside. At this moment, the incident pulse has passed and the detected field is mainly the surface waves trapped on the bow-tie.

The dimensions and dielectric permittivity of the STO particle allow it to behave as a resonator, storing energy, and forming field oscillation inside the particle. These oscillations are manifested in the asymmetry with respect to the particle center at $x \sim 200\ \mu$m. The resonant nature of the STO particle causes the local large field observed in the particle region Figs. 2(c) and 2(d). However, one should not misleadingly quantify the enhancement by comparing the fields right on top and outside the STO particle. The strength of the detected field (alternatively, the detection sensitivity) depends on the position of the NF probe. For the fixed $z \sim 25\ \mu$m, the sub-wavelength aperture is at different distances from the surface of the STO particle and the bow-tie antenna.

Based on the experimental observations, the main effects of the particle are (1) the destruction of the antenna field pattern symmetry and (2) the local modification of the electric field distribution near the particle. Note that even though the illumination is not completely symmetric (Fig. 2(b)) and, thus, it may induce some asymmetry in the antenna field pattern, the energy stays within the particle, causing the asymmetry to be more pronounced after $t \sim 1$ ps. Therefore, we conclude that the particle is the major contributor to the asymmetry. We also note that the effects of the particle become weaker as the distance between the antenna surface and the probe surface is increased, corresponding to the evanescent nature of the field induced by the sub-wavelength particle and reduction of the field concentration.

In our second experiment, the physical dimensions of the particle are reduced further to explore the effect of a particle with physical cross-section much smaller than the bow-tie arm area (~1/100). A TiO_2 sphere of radius $r \sim 15\ \mu$m and the relative permittivity $\varepsilon_r = 94 + 2.35$i (Refs. 20 and 21) is placed on another sample with the same bow-tie dimensions. The fundamental Mie resonance of this particle is expected at ~1.02 THz with a full width at half maximum of ~50 GHz for the power spectral line. The incident THz beam size in this experiment is slightly larger (formed by a waveguide with diameter Ø1.6 mm) to minimize the effect of misalignment of the incident field with the bow-tie center. The incident pulse, measured by the probe in the area outside the bow-tie ($x = 0$, $y = 150\ \mu$m) is shown in Fig. 3. An optical image of the sample and an example of the local THz field distribution in the region of the TiO_2 sphere are shown in the inset of Fig. 4.

The arrival time of the fundamental waveguide mode, which triggers the excitation of the Z-TSWs on the antenna edges, occurs at $t \sim 0.2$ ps and the incident pulse peaks at $t \sim 1.6$ ps. Spatial field distribution (*xy*-maps) measured at different time delays show that the particle becomes noticeable after the Z-TSWs have been formed on the bow-tie surface. In Fig. 4(a) ($t = 2.2$ ps) some perturbation of the field due to the particle is shown in the horizontal and vertical line scans taken at the position of the particle. The localized field perturbation is more pronounced at $t = 3.6$ ps (Fig. 4(c)). It agrees remarkably well with the dimensions of the TiO_2 particle, confirming that the particle is responsible for the localized disturbance of the field on the sub-wavelength scale. This conclusion is also supported by examining the *xy*-map of the same area of the bow-tie for the case of no particle present (Fig. 4(e)).

To evaluate the effect of the particle on the time-domain waveforms of the detected field, 23 ps long waveforms were recorded at three locations near another TiO_2 sphere of

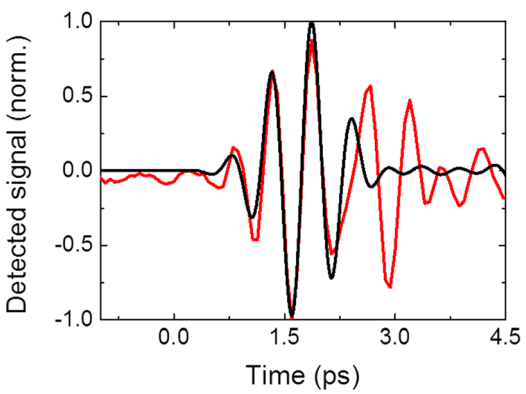

FIG. 3. Incident pulse waveform detected by the probe (red) outside the antenna area $(x,y) = (0, +150\ \mu$m). Note: (0,0) corresponds to the centre of the bow-tie. The black solid line shows a waveform of the pulse used in numerical calculations.

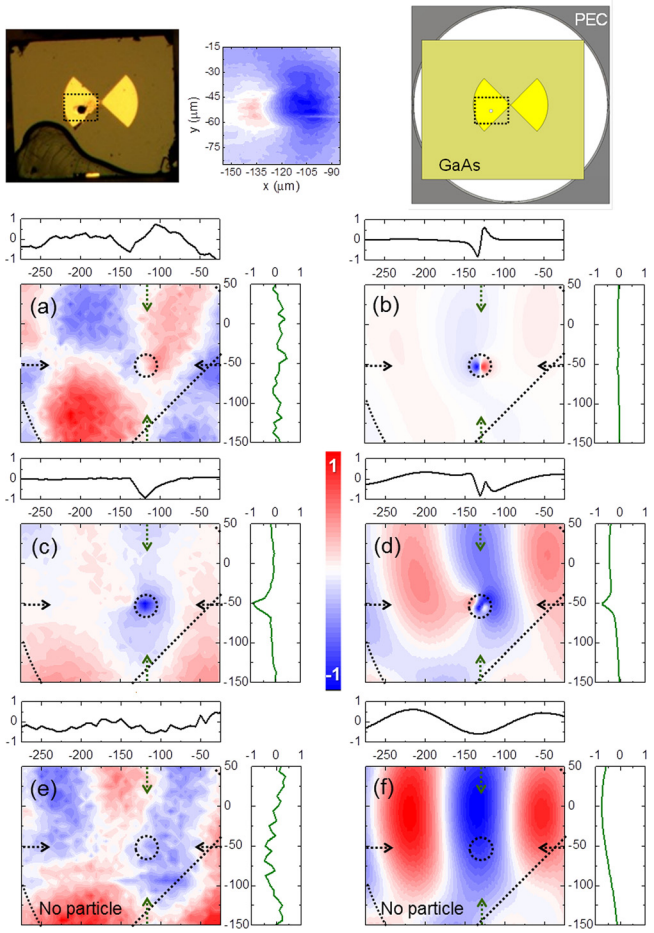

FIG. 4. Top insets: photograph of the sample (left), experimental, dE_x/dt and dE_z/dx, *xy*-map (instantaneous field, normalized) for $z = 31\ \mu$m at $t = 3.60$ ps, and sketch of the simulated structure (right). (a)-(f) Experimental, dE_x/dt and dE_z/dx (left column) and simulated, dE_z/dx (right column) *xy*-maps (instantaneous field, normalized) for $z = 31\ \mu$m at $t = 2.20$ ps (a), (b), 3.18 ps (d), (f), and 3.60 ps (c), (e). Notice that within the bow-tie region, the experimental data are simplified to dE_z/dx, and thus it can be compared with the simulations. Vertical green and horizontal black dotted arrows indicate the position of line scans plotted on the right-hand side and above each *xy*-map. The bow-tie geometry and the TiO_2 particle are outlined by black dotted lines and circles. (e), (f) Show maps of the same area for the bow-tie without the particle.

similar size placed at the same position on the same bow-tie (Fig. 4, top inset).[24] The sphere noticeably affects the amplitude of the detected field; see Fig. 4, top inset. The effect of the sphere on the time-domain waveform is more complex (see supplementary material[24]), as the waveforms and the corresponding spectra represent a superposition of several modes of the bow-tie. We note however, that in this configuration we cannot identify long-lasting oscillations of the field expected for the Mie resonance of the particle, which in theory, should persist for ~7 ps.

To confirm our findings and to explore the nature of the observed effects, we model this experiment using the finite-integration-method-based CST Microwave Studio™ and its transient solver akin to our previous work.[4] The dimensions of the substrate, the bow-tie and TiO_2 particle are determined from the optical microscope images (top left inset of Fig. 4) and used in the calculations.[24] The incident field in the calculations is matched to the experimentally measured waveform in Fig. 3 to ensure that modelled results corresponds the experimental conditions.[3,4] The front part of the waveform corresponds to the dominant waveguide mode. Note that at later times (beyond 2.5 ps), there is a contribution due to a higher order waveguide mode and scattering from the sample edges, which arrive delayed.

The numerical calculations, shown in the right column of Fig. 4, reproduce the localized field near the particle, detected at the time corresponding to the peak of the incident pulse (at $t = 2.20$ ps) and just after the pulse ($t = 3.18$ ps). When the particle is not present, the localized field distribution disappears in Fig. 4(f), as it happens in the experiment (Fig. 4(e)). This corroborates that the sub-wavelength particle is indeed responsible for the measured field distortion. Given the negligible amplitude of the horizontal components, $E_{x,y}$, developed near the particle compared to the normal component, E_z (according to the modelling they are at least one order of magnitude lower), Fig. 4(b), 4(d), 4(f) show only the effect of the E_z component. Notice, however, that the numerical calculations can resolve very small features displayed within the particle that the NF probe cannot distinguish given its aperture-size-governed resolution; see Figs. 4(c) and 4(d). Also, the simulations can quantify directly the field strength at inaccessible position for the NF probe like inside the particle. Therefore, a combined experimental and computation approach can become a powerful analytical tool.

From the experimental point of view, the optimal shape of the Z-TSW supporting metallic pattern is subject to further discussion. As it is discussed in the supplementary material,[24] the present configuration involves the interaction of multiple Z-TSWs induced by the fundamental waveguide mode and higher-order modes. The complex spectrum obtained is difficult to interpret. We envision that a tapered metallic strip could ease the experiment and facilitate the spectroscopy analysis by simplifying the Z-TSW distribution. By illuminating the wider end of the strip (with a spot smaller than the width of the strip, but partially blocked by the strip), only Z-TSWs propagating in one direction along the strip will be induced, eliminating the interference patterns seen for instance in the bow-ties.[3,4,26] On the other hand, a resonant antenna can improve sensitivity of this method for THz spectroscopy, albeit at the expense of the bandwidth.

Particles with a flat surface (such as the first sample used here) are likely to produce a stronger signal compared to rounded particles (such as the second sample) due to the fact that only the apex of the rounded particle can be in close proximity to the probe. This is especially critical when the particle is much smaller than the wavelength and the induced polarization of the particle decays quickly with the distance from the particle. As a final remark, particles with lower ε_r than those studied here (which are already challenging for competing methods) can potentially be investigated with our proposed method, since it is sensitive to the impedance mismatch generated in the path of the Z-TSWs by the particle, rather than to the excitation of Mie resonances. However, the interaction between the particle and the interrogating Z-TSW would be reduced, deteriorating inevitably the sensitivity.

In conclusion, we have investigated the potential of Z-TSWs for imaging of sub-wavelength particles. As a proof of principle, we have demonstrated the effect of

sub-wavelength particles with large ε_r (STO and TiO_2) on Z-TSWs supported by a bow-tie antenna. In this NF probe configuration, a single particle as small as 30 μm noticeably distorts the detected THz field. We anticipate that this experimental configuration can be utilized for THz imaging of sub-wavelength objects, including those with low ε_r, whose physical cross-sections are not smaller than the NF aperture, and for spectroscopy analysis of these particles when a different Z-TSW-supporting geometry is used.

The authors gratefully acknowledge the group of Professor J. A. Harrington from Rutgers University for supplying the cylindrical waveguides, U.-C. Chung, C. Elissalde, and M. Maglione from Institut de Chimie de la Matière Condensée de Bordeaux (ICMCB), CNRS–UPR9048, for processing and providing TiO_2 microspheres, and J.-P. Guillet from LOMA for useful discussions. This work was supported by the Royal Society [Grant No. UF080745] and Engineering and Physical Sciences Research Council [Grant No. EP/G033870/1]. M. Navarro-Cía was supported by the Imperial College Junior Research Fellowship.

[1]C. A. Balanis, *Antenna Theory: Analysis and Design*, 3rd ed. (John Wiley & Sons, Inc., Hoboken, NJ, 2005).
[2]P. Bharadwaj, B. Deutsch, and L. Novotny, Adv. Opt. Photon. **1**, 438 (2009).
[3]R. Mueckstein, C. Graham, C. C. Renaud, A. J. Seeds, J. A. Harrington, and O. Mitrofanov, J. Infrared Millim. Waves **32**, 1031 (2011).
[4]M. Natrella, O. Mitrofanov, R. Mueckstein, C. Graham, C. C. Renaud, and A. J. Seeds, Opt. Express **20**, 16023 (2012).
[5]C. F. Bohren and D. R. Huffman, *Absorption and Scattering of Light by Small Particles* (John Wiley & Sons, Inc., New York, 1998).
[6]J. S. Melinger, N. Laman, S. Sree Harsha, and D. Grischkowsky, Appl. Phys. Lett. **89**, 251110 (2006).
[7]R. Mendis, V. Astley, J. Liu, and D. M. Mittleman, Appl. Phys. Lett. **95**, 171113 (2009).
[8]N. Klein, P. Lahl, U. Poppe, F. Kadlec, and P. Kužel, J. Appl. Phys. **98**, 014910 (2005).
[9]M. Theuer, R. Beigang, and D. Grischkowsky, Opt. Express **18**, 11456 (2010).
[10]J. Liu, R. Mendis, D. M. Mittleman, and N. Sakoda, Appl. Phys. Lett. **100**, 031101 (2012).
[11]O. Mitrofanov, C. C. Renaud, and A. J. Seeds, Opt. Express **20**, 6197 (2012).
[12]T. Akalin, A. Treizebré, and B. Bocquet, IEEE Trans. Microwave Theory Tech. **54**, 2762 (2006).
[13]J. Cunningham, M. B. Byrne, C. D. Wood and L. Dazhang, Electron. Lett. **46**, s34 (2010).
[14]M. A. Seo, H. R. Park, S. M. Koo, D. J. Park, J. H. Kang, O. K. Suwal, S. S. Choi, P. C. M. Planken, G. S. Park, N. K. Park, Q. H. Park, and D. S. Kim, Nature Photon. **3**, 152 (2009).
[15]J. R. Knab, A. J. L. Adam, E. Shaner, H. J. A. J. Starmans, and P. C. M. Planken, Opt. Express **21**, 1101 (2013).
[16]A. Doi, F. Blanchard, H. Hirori, and K. Tanaka, Opt. Express **18**, 18419 (2010).
[17]C. A. Werley, K. Fan, A. C. Strikwerda, S. M. Teo, X. Zhang, R. D. Averitt, and K. A. Nelson, Opt. Express **20**, 8551 (2012).
[18]V. Skoromets, H. Němec, C. Kadlec, D. Fattakhova-Rohlfing, and P. Kužel, Appl. Phys. Lett. **102**, 241106 (2013).
[19]P. Kužel, C. Kadlec, F. Kadlec, J. Schubert, and G. Panaitov, Appl. Phys. Lett. **93**, 052910 (2008).
[20]K. Berdel, J. G. Rivas, P. H. Bolivar, P. de Maagt, and H. Kurz, IEEE Trans. Microwave Theory Tech. **53**, 1266 (2005).
[21]H. Němec, C. Kadlec, F. Kadlec, P. Kužel, R. Yahiaoui, U.-C. Chung, C. Elissalde, M. Maglione, and P. Mounaix, Appl. Phys. Lett. **100**, 061117 (2012).
[22]H. Němec, P. Kužel, F. Kadlec, C. Kadlec, R. Yahiaoui, and P. Mounaix, Phys. Rev. B **79**, 241108(R) (2009).
[23]O. Mitrofanov, M. Lee, J. W. P. Hsu, I. Brener, R. Harel, J. F. Federici, J. D. Wynn, L. N. Pfeiffer, and K. W. West, IEEE J. Sel. Top. Quantum Electron. **7**, 600 (2001).
[24]See supplementary material at http://dx.doi.org/10.1063/1.4836195 for the clarification of the waveguide excitation appropriateness, for technical details of the modelling, and for the spectroscopy analysis.
[25]B. Bowden, J. A. Harrington, and O. Mitrofanov, Appl. Phys. Lett. **93**, 181104 (2008).
[26]R. Mueckstein and O. Mitrofanov, Opt. Express **19**, 3212 (2011).
[27]O. Mitrofanov, T. Tan, P. R. Mark, B. Bowden, and J. A. Harrington, Appl. Phys. Lett. **94**, 171104 (2009).
[28]O. Mitrofanov, L. N. Pfeiffer, and K. W. West, Appl. Phys. Lett. **81**, 1579 (2002).
[29]P. Kužel and F. Kadlec, C. R. Physique **9**, 197 (2008).